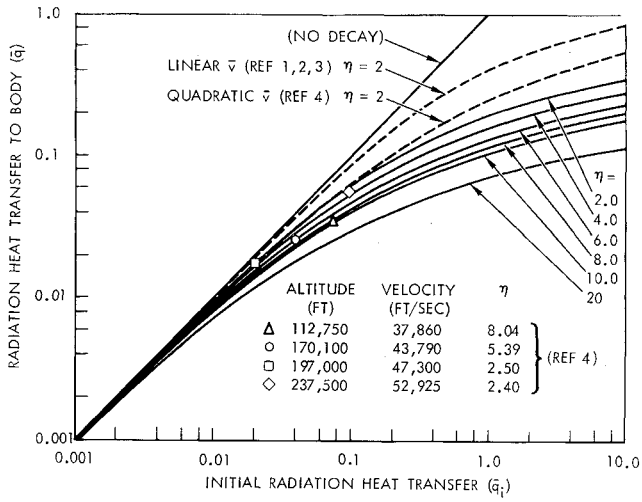

Fig. 2 Effect of decay on radiation heat transfer.

with the numerical results of Ref. 4. Substitution of Eq. (1) into the nonadiabatic energy equation, separation of variables, and integration yields the enthalpy profile in the form of

$$\bar{h} = \{1 + 4\bar{\delta}\bar{q}_i(\eta - 1)\ln[(\bar{y} - 2)/2(\bar{y} - 1)]\}^{1/(1-\eta)} \quad (2)$$

Use of Eq. (2) and the $\bar{\rho} = (\bar{h})^{-1}$ relationship defines the variation of density in the shock layer and, in turn, yields the velocity profile by means of Eq. (1).

An expression for the equilibrium radiation heat transfer to the stagnation point then can be derived easily using an assumed infinite plane radiating geometry and the previously described relationships, taking the form

$$\bar{q} = \bar{q}_i\bar{\delta}\int_0^1 \left\{1 + 4\bar{\delta}\bar{q}_i(\eta - 1)\ln\left[\frac{\bar{y} - 2}{2(\bar{y} - 1)}\right]\right\}^{\eta/(1-\eta)} d\bar{y} \quad (3)$$

The nondimensionalized shock-detachment distance is directly related to the calculation of $\bar{q}$. Therefore, using the results of Ref. 4 in connection with the relationships indicated in this note, $\bar{\delta}$ may be expressed as

$$\bar{\delta} = \int_0^1 \left\{1 + 4\bar{\delta}\bar{q}_i(\eta - 1)\ln\left[\frac{\bar{y} - 2}{2(\bar{y} - 1)}\right]\right\}^{1/(1-\eta)} d\bar{y} \quad (4)$$

Equations (3) and (4) were numerically integrated for various values of η and $\bar{q}_i$, and the results are shown in Figs. 2 and 3. Also shown for comparison are the results of radiative heat-transfer calculations assuming constant temperature and negligible effects of radiation absorption.

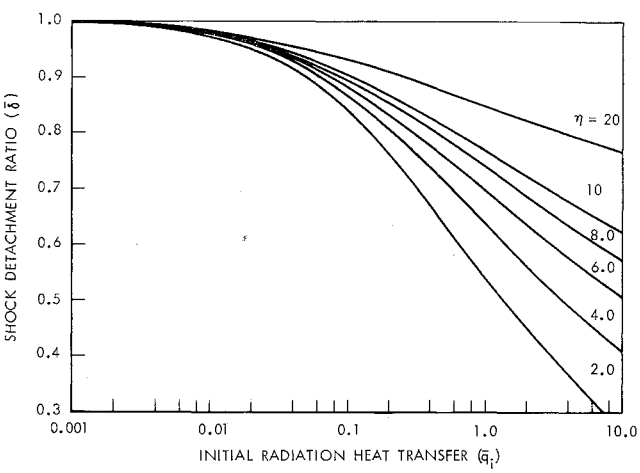

Fig. 3 Variation of shock-detachment distance with radiation heat-transfer parameter.

To demonstrate the resulting differences in the magnitude of the radiation heat transfer that evolve under the various assumed velocity profiles, computations were performed for $\eta = 2$, using a linear and quadratic velocity profile. These results were then compared with the results derived by using the $\bar{\rho}\bar{v}$ distribution contained in this note and are shown in Fig. 2. This comparison indicates that the use of a linear or quadratic velocity profile would yield considerably conservative heat-transfer results at relatively high values of $\bar{q}_i$ and justifies the use of the quadratic variation of $\bar{\rho}\bar{v}$ in the present analysis. The numerical solutions performed by the IBM 7094 program for a shock radius of 1 ft have been compared with the results of this approximate approach (Fig. 2), indicating excellent agreement.

References

[1] Hanley, G. M., Korkan, K. D., and Turner, S., "Manned Mars landing and return mission study," North American Aviation Space and Information Systems Division, First Quart. Rept., SID 63-1129 (August 1963).

[2] Goulard, R., "Preliminary estimates of radiative transfer effects on detached shock layers," AIAA J. 2, 494–502 (1964).

[3] Chin, J. H. and Hearne, L. F., "Shock-layer radiation for sphere-cones with radiative decay," AIAA J. 2, 1345–1347 (1964).

[4] Hanley, G. M. and Korkan, K. D., "Inviscid non-adiabatic flow in the stagnation region of blunt bodies," presented at the XVth International Astronautical Congress, Warsaw, Poland (September 1964).

Approximate Solution of Laminar Free Layers with Initial Thickness

JAMES E. HUBBARTT*
Georgia Institute of Technology, Atlanta, Ga.

NUMERICAL solutions of laminar free shear layers with finite initial thickness have been reported in Refs. 1 and 2. In the interest of providing a more convenient, approximate solution, Kubota and Dewey[3] explored the use of the momentum integral method using polynomial or exponential profiles. This note also explores the use of the momentum integral method but using similar velocity profiles. The initial layer is represented as a constant-pressure, similar profile that continues to develop in similarity downstream of the separation point as shown in Fig. 1 (inner profile). A constant-pressure, outer profile is considered to develop continuously upon the inner profile after separation. This outer profile is specified as a locally similar free layer determined by the velocity and velocity gradient (as an asymptotic limit) of the inner profile

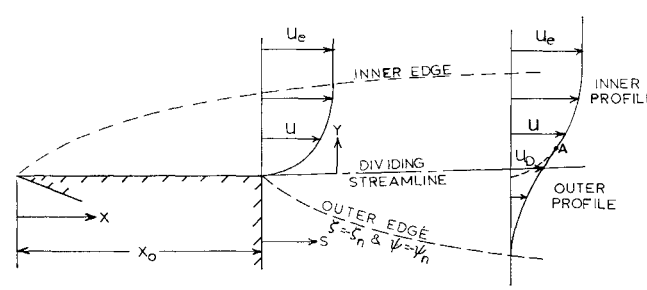

Fig. 1 Separated flow model.

Received November 20, 1964; revision received April 23, 1965. This work was partially supported under NASA Grant No. NSG-657.

* Associate Professor, School of Aerospace Engineering. Member AIAA.

at the matching point (A of Fig. 1). The complete family of profiles is established by choosing different matching points. The axial position for each member of this family of matched profiles is determined by satisfying a momentum integral balance.

Solution of Outer Profiles

The family of outer profiles is generated by similar solutions for the general case of a free shear layer developing on a constant-pressure, nonuniform stream. Assuming that $\mu/\mu_e = C(T/T_e)$, where subscript e represents a reference condition, the momentum and continuity equations may be combined to give[4]

$$\frac{\partial u/u_e}{\partial S^*} = \frac{\partial(u/u_e)(\partial u/u_e/\partial\Psi^*)}{\partial\Psi^*} \tag{1}$$

where $S^* = S/L$, $\Psi^* = \Psi/(C\nu_e u_e L)^{1/2}$, and L = reference length. Now express $u/u_e = (u/u_D)(u_D/u_e)$ where u_D is the velocity of the dividing streamline, and seek similar solutions for u/u_D. Employing

$$\zeta = \Psi^*(S^*)^{1/(\beta-2)} \qquad \frac{u_D}{u_e} = \frac{a\beta(S^*)^{\beta/(2-\beta)}}{2-\beta} \tag{2}$$

where a and β are arbitrary constants, Eq. (1) transforms to the following ordinary differential equation for the similar velocity profiles u/u_D:

$$-\frac{\zeta}{\beta}\frac{d(au/u_D)}{d\zeta} + \frac{au}{u_D} = \frac{1}{2}\frac{d^2(au/u_D)^2}{d\zeta^2} \tag{3}$$

The boundary conditions that may be satisfied are

$$y \to -\infty\colon\ u/u_D = 0 \qquad \zeta = 0\colon\ u/u_D = 1 \tag{4}$$

As $y \to -\infty$, ζ approaches a limit that will be indicated by $-\zeta_n$. After transforming Eq. (3) to the independent variable $\epsilon = (\zeta + \zeta_n)/\zeta_n$ a series solution in ϵ can be generated as illustrated in Ref. 5. To fifth order in ϵ the solution is

$$u/u_D = F(\beta, \epsilon)/F(\beta, 1) \tag{5}$$

where $\beta = (2a-1)/a$,

$$F(\beta,\epsilon) = \epsilon - 0.25(1-\beta)\epsilon^2 + 0.01389(1-\beta^2)\epsilon^2 + 0.00174(1-\beta^2)(1-2\beta)\epsilon^4 + 0.00015(1-\beta^2)[8\beta^2 - \tfrac{81}{11}\beta + 1]\epsilon^5$$

The similar profiles given by Eq. (5) are illustrated in Fig. 2. The parameter β determines the asymptotic limits for large ϵ. For $\beta = 0$, Eq. (5) reduces to the solution of Ref. 5 (i.e., a free layer developing on a uniform stream). In this case, the apparent singularity in Eq. (3) is removed (as required in order to obtain solutions other than the trivial solution $u = 0$) if one replaces $a\beta$ by a new finite constant C giving $u_D/u_e = C$. Equation (3) then reduces to the Blasius equation.

Although Eq. (5) converges rather rapidly, it cannot be employed to determine the velocity profiles for large values of ϵ. One can, however, evaluate the asymptotic solutions by considering the solution of Eq. (3) for large ζ. In this case the last term of Eq. (3) can be dropped in comparison with the other terms for $\beta < 1.0$, giving the simple solution

$$u/u_D \propto \zeta^\beta = \zeta_n{}^\beta(\epsilon - 1)^\beta \tag{6}$$

For present purposes it is convenient to evaluate β as required in Eq. (5) from this asymptotic solution. Equation (6) gives

$$[\zeta/(u/u_D)][d(u/u_D)/d\zeta] = \beta \tag{7}$$

For $\beta = 0$, Eq. (6) gives a uniform flow at large values of ϵ. For $\beta = \frac{1}{2}$, the asymptotic solution corresponds to a constant velocity gradient du/dY where Y is the transformed coordinate

$$Y = \int_0^y \frac{\rho}{\rho_e}\,dy$$

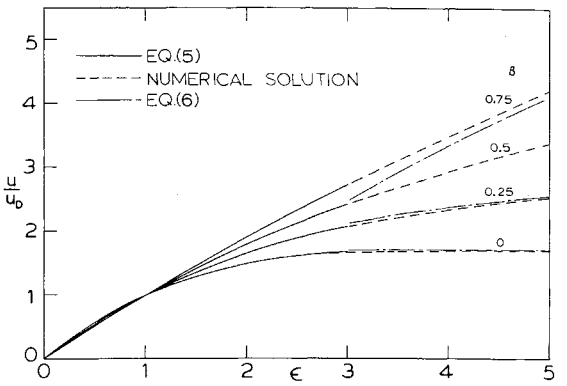

Fig. 2 Outer profiles.

This represents the starting solution for an initial Blasius profile as generated in Ref. 1.

In order to evaluate the accuracy of the series solution given by Eq. (5) and to determine the manner in which the solution approached the asymptotic limit, Eq. (3) was integrated numerically starting with the series solution at $\epsilon = 0.25$. The results are shown on Fig. 2. Clearly, the series solution is accurate to $\epsilon = 3$ for $0 < \beta < 0.75$. The asymptotic solution as determined by matching Eq. (6) to the numerical solution at large ϵ ($\epsilon = 10$) is also shown on Fig. 3. For $\beta = 0.5$ the asymptotic solution agrees with the numerical solution and, therefore, is omitted. For $0 < \beta < 0.5$, the asymptotic solution is essentially reached at $\epsilon = 3.0$ with maximum error in u/u_D of 3% at $\beta = 0.25$. Since the present study is primarily concerned with β in this range, it has been assumed that the asymptotic solution is obtained at $\epsilon = 3$.

Solution for Entire Shear Layer

The nondimensional velocity profiles for the entire shear layer are now represented by members of the family profiles given by Eq. (5) patched (matching u/u_e) to the initial similar profile at various matching points A. The matching point at $\epsilon = 3.0$ on the inner profile is considered to represent the asymptotic solution for the outer profile. Thus, β, which specifies each particular member of the outer profile, is evaluated from Eq. (7) applied to the inner profile at A. The axial position S is specified for each profile by the conservation of momentum.

The momentum equation for a free shear layer can be expressed in the form

$$d\theta^*/dS^* = d\Psi_n{}^*/dS^* \tag{8}$$

where $\theta^* = \theta(u_e/C\nu_e L)^{1/2}$ and θ is the transformed momentum

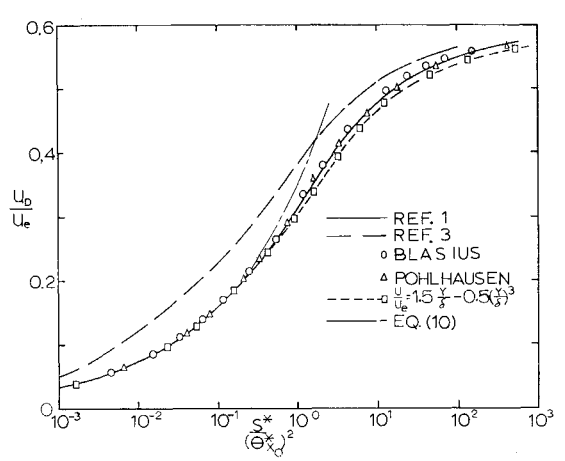

Fig. 3 Dividing streamline velocities for initial flat-plate profile.

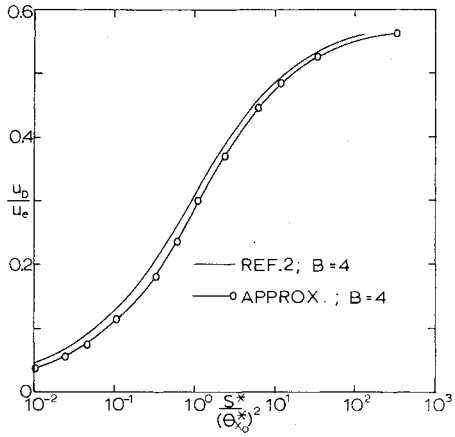

Fig. 4 Dividing streamline velocities for initial blowing profile.

thickness. Integrating from $x_0(S = 0)$ to S gives

$$\theta_{x_0}^* = \theta_s^* - \Psi_{ns}^* \tag{9}$$

(subscripts s and x_0 indicate conditions evaluated at S and x_0). Squaring, introducing $\Psi_{ns}^* = 0.5\Psi_{As}^*$ (i.e., for $\epsilon = 3.0$ at point A), and dividing by $(x_0^* + S^*)$, gives after some rearranging

$$S^*/(\theta_{x_0}^*)^2 = [\theta_s^*/(x_0^* + s^*)^{1/2} - 0.5\Psi_{As}^*/(x_0^* + S^*)^{1/2}]^{-2} - x_0^*/(\theta x_0^*)^2 \tag{10}$$

For constant-pressure similar inner profiles, the terms in this expression are independent of the shear layer scale. For any assumed inner profile and matching outer profile as specified by the matching point [specified by $\Psi_{As}^*/(x_0^* + S^*)^{1/2}$] the value of $(S^* + x_0^*)^{1/2}/\theta_s^*$ can be related to $\Psi_{As}^*/(x_0^* + S^*)^{1/2}$ using the definition of θ_1. $S^*/(\theta_{x0})^2$ is then evaluated from Eq. (10) for each matching point. The corresponding values of u_D/u_e are given by

$$u_D/u_e = (u_D/u_A)(u_A/u_e) = [F(\beta, 1)/F(\beta, 3)](u_A/u_e)$$

where u_D/u_A is expressed by Eq. (5), and u_A/u_e is given by each specified matching point.

The computed variations in u_D/u_e with $S^*/(\theta_{x0}^*)^2$ are shown in Fig. 3 for the flat-plate inner profile expressed by the Blasius solution, the Pohlhausen polynomial, and a cubic. Excellent agreement is obtained between these results and the exact numerical solution of Ref. 1. The approximate results of Ref. 3 are also shown for comparison. For small values of S, the velocity ratio u_D/u_e corresponds to that for a free layer developing on a nonuniform flow of constant velocity gradient. The solutions for small S and the Blasius and Pohlhausen profiles reduce approximately to the simple relation

$$u_D/u_e = 0.35[S^*/(\theta_{x0}^*)^2]^{1/3} \tag{11}$$

This equation is also plotted on Fig. 3 to show that it represents a reasonable approximation up to $u_D/u_e \approx 0.25$.

The shear layer velocity profiles have also been compared with those of Ref. 1 for an initial Blasius profile. Excellent agreement exists for $u_D/u_e \leqslant 0.40$. For higher values of u_D/u_e, the velocity gradients in the outer profile of the approximate solution become significantly less than those of Ref. 1 because matching becomes progressively more critical. The relative shape of the profiles are essentially correct, however. Thus, good agreement should be obtainable by either improving the matching or by satisfying the momentum equation for both the region of $\Psi > 0$ and $\Psi < 0$. The velocity of the dividing streamline is not sensitive to these differences, however.

Figure 4 shows a comparison of the approximate solution with the exact numerical solution of Ref. 2 for a rather extreme case of the surface blowing profiles of Ref. 6. In this case the present solution results in values of u_D/u_e which are slightly low (about 0.02 below the exact values). This may, in part, be due to the fact that the solution begins with $\beta > 0.50$ giving rise to a poorer asymptotic match at $\epsilon = 3$.

References

[1] Denison, M. R. and Baum, E., "Compressible free shear layer with finite initial thickness," AIAA J. **1**, 342–349 (1963).

[2] Baum, E., King, H. H., and Denison, M. R., "Recent studies of laminar base-flow region," AIAA J. **2**, 1527–1534 (1964).

[3] Kubota, T. and Dewey, C. F., Jr., "Momentum integral methods for the laminar free shear layer," AIAA J. **2**, 625–629 (1964).

[4] Chapman, D. R., "Theoretical analysis of heat transfer in regions of separated flow," NACA TN 3792 (1956).

[5] Hubbartt, J. E., "Integral solution for compressible laminar mixing," AIAA J. **2**, 1657–1659 (1964).

[6] Emmons, H. W. and Leigh, D. C., "Tabulation of the Blasius functions with blowing and suction," Great Britain Aeronautical Research Council TR C.P. 157 (1954).

Kinetic Energy and Angular Momentum about the Variable Center of Mass of a Satellite

BERTRAND T. FANG*
The Catholic University of America, Washington, D. C.

Nomenclature

$\{E\}$ = unit dyadic
$\mathbf{h}$ = angular momentum vector
$\{I\}$ = moment of inertia dyadic
m_j = mass of individual body
M = total mass of satellite
$\mathbf{R}_j$ = absolute position vector
$\mathbf{r}_j$ = relative position vector
t = time
T = kinetic energy
ω_j = angular velocity vector

Subscript

0 = satellite main body

IT is well known that the motion of a system of particles or rigid bodies can be conveniently separated into a motion of the center of mass of the system and a motion about the center of mass. When these two motions are uncoupled, considerable simplification results. In space applications, this means that the trajectory and attitude motions of a satellite can sometimes be treated separately. A satellite generally consists of a main body and many auxiliary bodies that have motions relative to the main body.† The relative motion of these smaller bodies often may be neglected in studying the orbital motion of the satellite. But frequently it is just the motion of these smaller masses which is responsible for the damping, stability, and instability of the attitude of a satellite. In these cases it is necessary to determine the total kinetic energy and angular momentum of the satellite about its center of mass, taking into consideration the motions of these smaller masses. Now, because of the motions

Received January 15, 1965; revision received April 27, 1965.

* Assistant Professor, Department of Space Science and Applied Physics. Member AIAA.

† A detailed derivation of the equations of motion of a multiple-part satellite may be found in Refs. 1 and 2.